

LOS and NLOS Channel Modeling for Terahertz Wireless Communication with Scattered Rays

Anamaria Moldovan¹, Michael A. Ruder¹, Ian F. Akyildiz², and Wolfgang H. Gerstacker¹

¹Institute for Digital Communications, Friedrich-Alexander-University Erlangen-Nürnberg (FAU),
Cauerstr. 7, D-91058 Erlangen, Germany, {moldovan, ruder, gersta}@LNT.de

²Broadband Wireless Networking Lab, Georgia Institute of Technology, Atlanta, USA, ian.akyildiz@ee.gatech.edu

Abstract—In this paper, the wireless communication over indoor Terahertz (THz) channels is studied. The physical mechanisms governing a wireless transmission in the 0.1 – 10 THz band are a very high molecular absorption and spreading loss which result in a very high and frequency-selective path loss for the line-of-sight (LOS) links. For the non-line-of-sight (NLOS) propagation, a very high reflection loss depending on the shape, material, and roughness of the reflecting surface affects the THz wave propagation. Taking these peculiarities of the THz radiation into account and applying a ray tracing approach for scattered rays, a novel deterministic equivalent channel model is developed that accounts for both the LOS and NLOS propagation cases. Furthermore, the channel capacity of the proposed model is investigated. Simulation results demonstrate that for distances, up to 1 m, data rates in the order of Terabit per second (Tbps) are obtained for a transmit power of 1 Watt. Moreover, the capacity of only the NLOS component is around 100 Gigabit per second (Gbps). These results are highly motivating to develop future wireless THz communication systems.

I. INTRODUCTION

To satisfy the growing demands for high data rates in wireless communication systems, the network capacity has been enhanced by increasing the spectral efficiency by means of advanced modulation schemes and signal processing techniques [1]. However, the efficiency of these methods is limited due to the narrow bandwidth of legacy systems. Another approach for throughput enhancement is increasing the operation frequency. In this respect significant effort is devoted to research in the field of millimeter-waves, which allow for data rates up to 10 Gigabit per second (Gbps) [2]. Yet, the increasing demand for even higher data rates in wireless communications will eventually lead to the allocation of wider bandwidths in the Terahertz (THz) frequency range. For this purpose, the IEEE 802.15 Terahertz Interest Group (IGthz) has been established in 2008 to explore the feasibility of the Terahertz band for wireless communications [3]. Since January 2014 there is an official IEEE standardization committee called 100Gbps.

The THz band, or so-called sub-millimeter band, covers the frequency range between 100 GHz and 10 THz, with corresponding wavelengths between 3 mm and 30 μm . In contrast to X-ray radiation, THz radiation is non-ionizing and therefore it can be used in close proximity to the human body. Other important advantages of THz radiation include the penetration of many opaque materials and the high selectivity due to the fact that many molecules have resonance frequencies within the THz band, enabling their detection when they are present.

Many applications of THz waves, some of them already available, like THz body scanners at airports or medical imaging, are based on these properties. So far, THz waves have not been utilized for wireless communications because of the lack of devices for generating and detecting them [1]. Currently,

though there are three major technologies such as *Silicon-Germanium* (SiGe), *Galium-Nitride* (GaN), and *Graphene* that are being considered for the development of ultra-high-speed transceivers in the THz band [4].

The physical mechanisms governing a wireless transmission in the THz band are different from those which affect schemes operating in the lower frequency bands where the propagation is mainly influenced by the spreading loss. Therefore, already existing channel models cannot be re-used for THz communications. The peculiarities of THz radiation are a very high *molecular absorption* and *spreading loss* which result in a very high and frequency-selective path loss for line-of-sight (LOS) links. For non-line-of-sight (NLOS) propagation, a very high *reflection loss* depending on the shape, material, and roughness of the reflecting surface governs the THz wave propagation.

So far, the existing literature on the channel modeling in the THz band is sparse. In [5], an LOS propagation model for the entire THz band was developed by analyzing the impact of molecular absorption on the path loss. To account for the NLOS propagation, it is necessary to characterize the reflection of electromagnetic (EM) waves at obstacles in the THz frequency range. The properties of typical indoor materials have been measured in the 0.1 to 1 THz frequency range [6], [7]. Furthermore, the scattering behavior of rough surfaces both in the specular [8] and non-specular [9], [10] directions has been analyzed at 300 GHz band. To this end, these works employ Kirchhoff scattering from rough surfaces theory [11].

The few existing channel models in the THz band [12], [13] characterize the multipath channel at 0.3 THz based on ray-tracing simulations. They are mainly based on measurements and consider specular reflections only.

In this paper, we propose a novel deterministic channel model for the 0.1 to 1 THz frequency range, based on Kirchhoff scattering theory and ray tracing that includes the effects of LOS and NLOS propagation. We improve the LOS propagation model proposed in [5] by adopting an updated molecular High Resolution Transmission (HITRAN) 2012 database and realistic values for the fraction of water vapor in the air. Our improved LOS propagation model in Section II shows a significantly lower molecular absorption loss as compared to [4]. For the NLOS propagation, in Section III we model the reflection loss as discussed in [10], including also the effects of the molecular absorption loss and spreading loss on the indirect paths. Furthermore, the channel capacity is determined in Section V by employing the proposed deterministic channel model for LOS and NLOS propagation from Section IV and optimizing the transmit power allocation via water-filling. Our simulation results show that for relatively short distances, up to 1 m, data rates in the order of Terabit per second (Tbps) can be obtained for a transmit power of 1 Watt. This result encourages the use of the THz band for wireless short range

interconnections among devices, for instance to transfer the content of a blue ray disk to a tablet in less than 1 second.

II. LINE-OF-SIGHT PROPAGATION

In [5], a propagation model for communications in the THz band for LOS conditions has been developed. This model accounts for the total path loss that an EM wave in the THz band suffers from due to absorption and spreading loss when propagating over very short distances. In the following, we further extend this channel model for LOS propagation.

In the THz band, the absorption level of atmospheric gases is very strong which is caused by molecular resonances primarily due to water vapor and oxygen. If the fraction of water in the air is q_{wv} , the fraction q_{dryAir} of the other gases in the air, referred to as dry air (air without water molecules) scales accordingly so that $q_{wv} + q_{dryAir} = 1$. In order to determine the amount of water molecules in the air, the relative humidity (RH) and the dew point temperature ($T_{\circ C}^{dew}$) are two widely used indicators. The *relative humidity* is commonly defined as the percentage of the actual water vapor dry mass mixing ratio q_{wv} to the saturation mixing ratio q_{sat} at the system temperature $T_{\circ C}$ and pressure p [14]

$$RH = 100 \frac{q_{wv}}{q_{sat}}. \quad (1)$$

The water vapor dry mass mixing ratio and the saturation mixing ratio are calculated as

$$q_{wv} = 0.622 \frac{p_{wv}}{p - p_{wv}} \text{ and } q_{sat} = 0.622 \frac{p_{sat}}{p - p_{sat}}, \quad (2)$$

respectively, where 0.622 is the ratio of the molecular weights of water and dry air, p_{wv} is actual water vapor pressure, and p_{sat} is the saturation vapor pressure. The temperature to which air must be cooled to become saturated is called *dew point temperature* $T_{\circ C}^{dew}$. Therefore, when the temperature of the system $T_{\circ C}$ equals the dew point temperature it means that the relative humidity RH is 100% and we can see condensation. To express RH in terms of $T_{\circ C}^{dew}$, an expression for the dependence of p_{sat} on $T_{\circ C}$ is needed. One of the most widely used, highly accurate empirical expressions is

$$p_{sat} = K_1 \exp\left(\frac{K_2 \cdot T_{\circ C}}{K_3 + T_{\circ C}}\right), \quad (3)$$

which is commonly referred to as the Magnus formula [14]. The constants $K_1 = 610.94$ Pa, $K_2 = 17.625$, $K_3 = 243.04$ °C were obtained by measurements [14].

By using the Magnus formula in (2), we can determine the fraction of water molecules at saturation q_{sat} . For finding the fraction of water molecules at $RH \neq 100\%$, q_{wv} is computed from (1) which is finally used to obtain the mixing ratio of the individual gases.

The molecules absorb and emit radiation at certain discrete frequencies corresponding to allowable changes in their quantum energy levels. These energies correspond to a specific frequency f according to $E = \hbar \cdot f$, where $\hbar = 6.6262 \times 10^{-34}$ [Js] is the Planck's constant. For all other frequencies, the molecule is non-absorbing. Taking this into account, we obtain the absorption cross-section, as a function of the wave frequency for the considered molecule, resulting in an *absorption line spectrum*.

We need three parameters to compute the cross-section of an absorption line under a given set of environmental conditions:

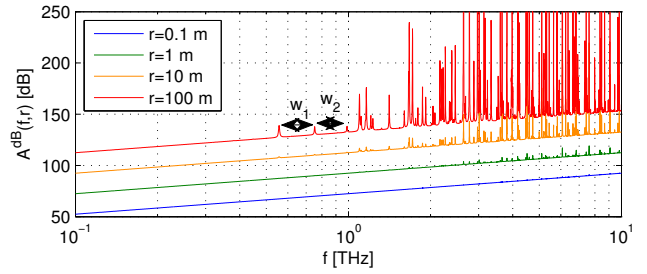


Figure 1. LOS path loss vs. frequency for normal conditions, $T_{\circ C} = 23^{\circ}C$, $RH = 40\%$, $q_{wv} = 0.7\%$.

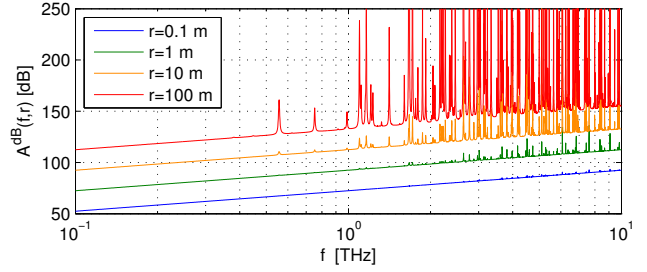


Figure 2. LOS path loss vs. frequency for tropical conditions, $T_{\circ C} = 30^{\circ}C$, $RH = 100\%$, and $q_{wv} = 2.7\%$.

line position, line intensity, and line shape, all computed in [5]. The molecular absorption coefficient $\alpha_{molec}(f, T_K, p)$ subsumes the influence of these parameters on the absorption, and it is calculated according to [5], where T_K stands for the system temperature in Kelvin.

The total attenuation that an EM wave of a frequency f suffers from due to molecular absorption when traveling over a distance r is given by

$$A_{abs}(f, r) = e^{\alpha_{molec}(f, T_K, p)r}. \quad (4)$$

To derive the molecular absorption coefficient we compute the fraction of water in the air based on Magnus formula while invoking HITRAN 2012 [15]. The (free space) spreading loss accounts for the loss due to the expansion of the wave as it propagates through the medium [5],

$$A_{spread}^{dB}(f, r) = 20 \log_{10} \left(\frac{4\pi fr}{c} \right), \quad (5)$$

where $c = 2.9979 \times 10^8$ [m/s] is the speed of light. The total path loss can be expressed as the sum of the molecular absorption loss and spreading loss in dB [5]

$$\begin{aligned} A^{dB}(f, r) &= A_{spread}^{dB}(f, r) + A_{abs}^{dB}(f, r) \\ &= 20 \log_{10} \left(\frac{4\pi fr}{c} \right) + \alpha_{molec}(f, T_K, p) r 10 \log_{10} e. \end{aligned} \quad (6)$$

The LOS propagation channel loss in the THz band is illustrated in Figs. 1 and 2 for different concentrations of water vapor molecules, considering realistic environmental conditions, i.e., normal and tropical climate.

Our further developed LOS propagation model shows somewhat modified results as compared to [4]. We obtain a significantly lower molecular absorption loss that theoretically allows us to transmit over the entire THz bandwidth, for distances in the order of a few meters, as opposed to a transmission window of width 0.4 THz, with a center frequency of around 0.3 THz defined in [4]. Moreover, the transmission windows enabled by the molecular absorption are defined in [4]

at lower center frequencies due to higher molecular absorption loss.

III. NON-LINE-OF-SIGHT PROPAGATION

In an indoor scenario, the LOS propagation might be blocked by the presence of obstacles like moving people, furniture, or many diverse objects. In this case, the NLOS propagation will play an important role for enabling a stable wireless transmission. Therefore, it is mandatory to characterize the reflection properties of typical indoor building materials and to model the scattering of the EM waves at rough surfaces in the THz band by means of Kirchhoff scattering theory [11]. Without loss of generality, the incident electric field E_1 is assumed to be of unit amplitude in the following derivations [11].

The figures of merit which describe a rough surface are the roughness of the surface σ_{h_s} and the correlation length l_{corr} , i.e., the distance where the autocorrelation function has decayed to $\frac{1}{e}$ compared to its maximum [16]. These two parameters are obtained by measurements [6], [7].

The characteristics of the reflection are governed by the scattering coefficient, which is defined as [11]

$$\rho = \frac{E_2}{E_{20}}, \quad (8)$$

where E_2 is the scattered electric field and E_{20} is the electric field reflected in the direction of the specular reflection by a smooth, perfectly conducting surface. Specular means that the incident angle θ_1 , i.e., the angle between the incident ray and the surface normal, equals the reflected angle θ_2 , i.e., the angle between the reflected ray and the normal of the surface, and the angle θ_3 , defined for scattering directions that lie outside the plane of incidence (x, z) equals to zero. Since ρ is a complex quantity, it is necessary to determine the mean value of $|\rho|^2$,

$$\mathbb{E}\{|\rho|^2\} = \mathbb{E}\{\rho\rho^*\} = \frac{\mathbb{E}\{E_2E_2^*\}}{|E_{20}|^2}, \quad (9)$$

where $(\cdot)^*$ denotes the complex conjugate, and $\mathbb{E}\{\cdot\}$ refers to expectation, performed here over the surface area. Based on the *Helmholtz integral* [11, Appendix A] we obtain

$$E_{20} = \frac{j\gamma e^{j\gamma r_0} A \cos \theta_1}{2\pi r_0}, \quad (10)$$

where $\gamma = \frac{f}{2\pi c}$ is the propagation constant, A is the area of the scattering surface with dimensions X and Y , i.e., $A = X \cdot Y$, and θ_1 is the incident angle.

Assuming an infinitely conductive surface, the average scattering coefficient of an incident wave on a rough surface under an angle θ_1 , scattered in the direction given by the angles θ_2 and θ_3 is computed as [11]

$$\mathbb{E}\{\rho\rho^*\}_\infty = e^{-g} \left(\rho_0^2 + \frac{\pi l_{\text{corr}}^2 F^2}{A} \sum_{m=1}^{\infty} \frac{g^m}{m!m} e^{-v_{xy}^2 l_{\text{corr}}^2 / (4m)} \right), \quad (11)$$

with $g = \sigma_{h_s}^2 v_z^2 = \sigma_{h_s}^2 (2\pi f/c)^2 (\cos \theta_1 + \cos \theta_2)^2$, $\rho_0 = \text{sinc}(v_x X) \cdot \text{sinc}(v_y Y)$, $v_x = (2\pi f/c)(\sin \theta_1 - \sin \theta_2 \cos \theta_3)$, $v_y = (2\pi f/c)(-\sin \theta_2 \sin \theta_3)$, $v_{xy} = \sqrt{v_x^2 + v_y^2}$, and

$$F = \frac{1 + \cos \theta_1 \cos \theta_2 - \sin \theta_1 \sin \theta_2 \cos \theta_3}{\cos \theta_1 (\cos \theta_1 + \cos \theta_2)}. \quad (12)$$

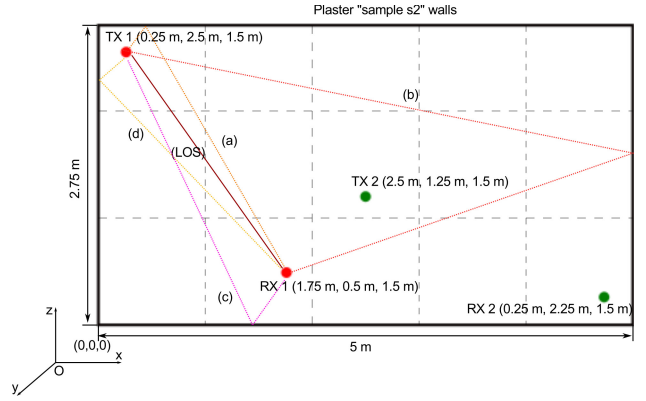


Figure 3. A deterministic indoor scenario with two arbitrary TX/RX positions

From (11) we observe that the mean scattering coefficient is the sum of two terms. The first term $e^{-g}\rho_0^2$ is the *specular spike* component of the specular reflection, whereas the second term in (11) corresponds to the *specular lobe*, i.e., the diffusely scattered field that results from the roughness of the surface and is distributed around the specular spike. For small values of g the specular spike is very strong. As the roughness measure g increases, the magnitude of the lobe component increases relative to the spike component.

Equation (11) is valid for a surface which is assumed to be a perfect conductor. In order to approximate the mean scattering coefficient for finite conductors, we average the Fresnel reflection coefficient Γ over the entire surface area and utilize the resulting value $\mathbb{E}\{\Gamma\Gamma^*\}$ as a constant in the Helmholtz integral [16]. Therefore, the scattering coefficient for finite conducting surfaces is obtained as

$$\mathbb{E}\{\rho\rho^*\}_{\text{finite}} = \mathbb{E}\{\Gamma\Gamma^*\}\mathbb{E}\{\rho\rho^*\}_\infty. \quad (13)$$

The mean scattered power is obtained as $\mathbb{E}\{P_2\} = \frac{1}{2}Y_0\mathbb{E}\{E_2E_2^*\}$ [11], while the incident power is $\mathbb{E}\{P_1\} = \frac{1}{2}Y_0|E_1|^2$, where $Y_0 = \frac{1}{120\pi}$ [S] is the admittance of free space.

Taking all these definitions into consideration, the average power reflection coefficient of a surface area A , describing the scattered power in a distance r_0 with respect to the incident power P_1 , is given by

$$\mathbb{E}\{R_{\text{power}}\} = \frac{\mathbb{E}\{P_2\}}{\mathbb{E}\{P_1\}} = |E_{20}|^2 \mathbb{E}\{\rho\rho^*\}_{\text{finite}}. \quad (14)$$

Substituting the value of E_{20} from (10) results in

$$\mathbb{E}\{R_{\text{power}}\} = \left(\frac{fA \cos \theta_1}{c r_0} \right)^2 \mathbb{E}\{\rho\rho^*\}_{\text{finite}}. \quad (15)$$

The non-specular scattering from rough surfaces will influence the broadband channel behavior [10]. This effect can be investigated by ray tracing simulations. In the following, the practical implementation of the Kirchhoff model in a ray tracing algorithm is discussed. An omnidirectional antenna is assumed. Using (15), the scattered power for arbitrary positions of the TX and of the RX can be computed. The simulation scenario consists of a small rectangular office room (length \times width \times height: 5 m \times 2.75 m \times 2.5 m), which is depicted in Fig. 3. The walls of the room are covered with plaster “sample s2” from [8] which has a high roughness. Reflections from

the floor and from the ceiling are neglected. The operational frequency range is 0.1 to 1 THz. For this realistic indoor environment, applying the Kirchhoff scattering theory for only a single scattering point on the whole surface of the wall is not a reasonable approach. First, in order for (15) to hold, the plane waves are assumed for both the incident and scattered electric fields. This is well justified if the source and the observation point are at a great distance from the surface as compared to the physical dimensions of the surface. Moreover, the received power is obtained by summing up the contributions of all the rays scattered from all over the surface area. If we apply the calculation just for a single scattering point then this does not allow for a broadband channel characterization, as only a single path is computed for each scattering plane [10]. Therefore, we employ a ray tracing algorithm such as proposed in [9] and [10]. This means that the entire surface area $A = X \cdot Y$, is separated into smaller square tiles. For each tile, we compute the powers of the rays scattered from the tile according to Kirchhoff equations, which are then summed up in order to obtain the total scattered power [9].

IV. EQUIVALENT CHANNEL MODEL

Based on all the previous observations, we can propose an equivalent deterministic channel model for an indoor environment, which captures the direct ray as well as indirect (or reflected) rays from rough surface scattering.

The equivalent channel transfer function is given by

$$H^{\text{EQ}}(f, r, \zeta) = H^{\text{LOS}}(f, r) e^{-j2\pi f \tau_{\text{LOS}}} + \sum_{i=1}^{M_{\text{rays}}} H_i^{\text{NLOS}}(f, \zeta_i) e^{-j2\pi f \tau_{\text{NLOS}_i}}, \quad (16)$$

where M_{rays} is the number of indirect rays, $\tau_{\text{LOS}} = r/c$ and $\tau_{\text{NLOS}_i} = \frac{r_{i1} + r_{i2}}{c}$ are the propagation delays of the LOS path and i^{th} NLOS path, respectively, with r denoting the distance between the TX and RX, r_{i1} the distance between the TX and the i^{th} scattering point and r_{i2} is the distance between the i^{th} scattering point and the RX. The vector $\zeta = [\zeta_1, \dots, \zeta_{M_{\text{rays}}}]$ describes the coordinates of all the scattering points, where $\zeta_i = [r_{i1}, r_{i2}, \theta_{i1}, \theta_{i2}, \theta_{i3}]$ defines the parameters of the i^{th} scattering point location.

The magnitude of the LOS path $H^{\text{LOS}}(f, r)$ following from (6) and (7) is

$$H^{\text{LOS}}(f, r) = H_{\text{spread}}(f, r) \cdot H_{\text{abs}}(f, r), \quad (17)$$

with

$$H_{\text{spread}}(f, r) = \frac{c}{4\pi \cdot f \cdot r}, \quad (18)$$

$$H_{\text{abs}}(f, r) = e^{-\frac{1}{2} \alpha_{\text{molec}}(f, T_{\text{K}}, p) r}. \quad (19)$$

The i^{th} NLOS path coefficient is defined as

$$H_i^{\text{NLOS}}(f, r, \zeta_i) = H_{\text{refl},i}(f, r_{i2}, \theta_{i1}, \theta_{i2}, \theta_{i3}) \times H_{\text{spread},i}(f, r_{i1}, r_{i2}) \cdot H_{\text{abs},i}(f, r_{i1}, r_{i2}), \quad (20)$$

with

$$H_{\text{refl},i}(f, r_{i2}, \theta_{i1}, \theta_{i2}, \theta_{i3}) = \sqrt{\mathbb{E}\{R_{\text{power},i}(f, r_{i2}, \theta_{i1}, \theta_{i2}, \theta_{i3})\}}, \quad (21)$$

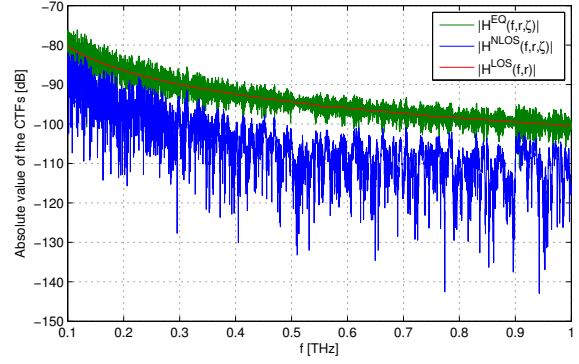


Figure 4. CTF for TX/RX position 1.

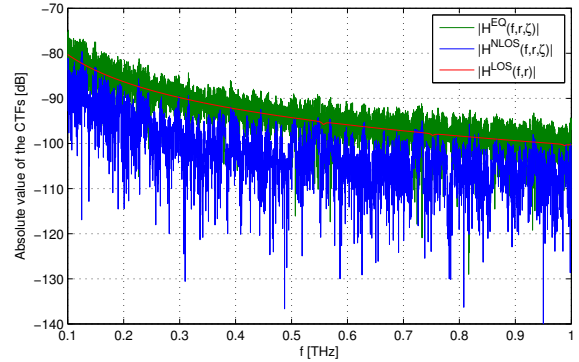


Figure 5. CTF for TX/RX position 2.

$$H_{\text{spread},i}(f, r_{i1}, r_{i2}) = \frac{c}{4\pi \cdot f \cdot (r_{i1} + r_{i2})}, \quad (22)$$

$$H_{\text{abs},i}(f, r_{i1}, r_{i2}) = e^{-\frac{1}{2} \alpha_{\text{molec}}(f, T_{\text{K}}, p)(r_{i1} + r_{i2})}. \quad (23)$$

The equivalent channel transfer function (CTF) highly depends on the geometry of the specific propagation environment, i.e., the position of the TX and RX. We chose two positions for the TX/RX as shown in Fig. 3. Both positions have the same LOS component, i.e., the distance between the TX and RX is the same and equals $r = 2.5$ m. In Figs. 4 and 5 the magnitude of the equivalent CTFs of the considered scenarios are depicted. Due to the constructive and destructive superposition of the numerous reflected paths and the direct path, fluctuations of the CTFs are observed. Yet, for both scenarios the LOS component dominates and exhibits over the entire band from 0.1 THz to 1 THz a path gain of -80 dB to -100 dB, respectively. For TX/RX position 2, at certain discrete frequencies the NLOS gain is slightly larger than the LOS gain. This is because of the constructive interference of the multiple indirect paths.

V. CAPACITY ANALYSIS

In order to quantify the performance of the proposed system in the 0.1 to 1 THz range, we use the channel capacity as a metric. The channel transfer function $H^{\text{EQ}}(f, r, \zeta)$ is highly frequency selective. Therefore, we divide the total bandwidth B into N narrow sub-bands of equal width $\Delta f = \frac{B}{N}$. If Δf is small enough, each subchannel can be modeled as frequency non-selective [5]. By summing over the individual capacities of each sub-band we obtain the total channel capacity in [bps] as

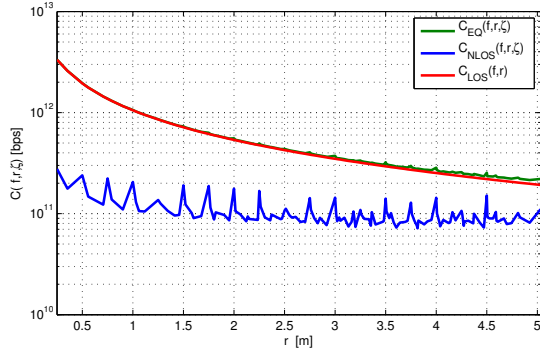


Figure 6. Average capacity of the LOS, NLOS, and EQ components as a function of the distance between TX and RX, for $P = 1$ W.

$$C(f, r, \zeta) = \Delta f \sum_{i=1}^N \log_2 \left(1 + \frac{\Phi_T(f_i, r, \zeta) |H^{\text{EQ}}(f_i, r, \zeta)|^2}{\Phi_N(f_i)} \right) \quad (24)$$

where $\Phi_T(f, r, \zeta)$ is the power spectral density (PSD) of the transmitted signal, $H^{\text{EQ}}(f, r, \zeta)$ is the equivalent channel factor and $\Phi_N(f)$ is the noise PSD, which is given for high frequencies [17] by

$$\Phi_N(f) = \frac{\hbar f}{\exp\left(\frac{\hbar f}{k_B T_K^0}\right) - 1}, \quad (25)$$

and assumed flat in the considered sub-bands. Here, $k_B = 1.3806 \times 10^{-23}$ [J/K] denotes Boltzmann's constant.

For the transmit signal we perform optimal power allocation in order to maximize the channel capacity. Therefore, the PSD of the transmitted signal is chosen such that it satisfies the water-filling condition [18]

$$\Phi_T^{\text{opt}}(f_i, r, \zeta) = \left[\mu - \frac{\Phi_N(f_i)}{|H^{\text{EQ}}(f_i, r, \zeta)|^2} \right]^+, \quad (26)$$

where $[x]^+ = \max\{0, x\}$ and the water level μ is computed such that

$$\Delta f \cdot \left(\sum_{i=1}^N \left[\mu - \frac{\Phi_N(f_i)}{|H^{\text{EQ}}(f_i, r, \zeta)|^2} \right]^+ \right) = P, \quad (27)$$

with the total transmit power P . A typical transmit power for THz frequencies is between 1 mW and 1 W.

To compute the average capacity, we vary the position of the TX as well as that of the RX in steps of $\Delta x = \Delta y = 0.25$ m for a fixed distance. Numerical results indicate that for $P = 1$ W, Tbps rates can be achieved for distances up to 1 m as depicted in Fig. 6. Moreover, we observe that the LOS component dominates the performance. At large distances the results reveal that the NLOS component becomes more and more important. It should be noted that the capacity of only the NLOS component is around 100 Gbps if water-filling is performed for the pure NLOS case. These results encourage the development of future indoor THz communication systems.

VI. CONCLUSIONS

In this paper, we have studied the problem of wireless communications over Terahertz (THz) channels. We have analyzed the impact of the molecular absorption loss and the

reflection loss on LOS and NLOS propagation, respectively. Including these peculiarities of the THz radiation and based on Kirchhoff scattering theory and ray tracing simulations we have derived a deterministic equivalent indoor channel model for both the LOS and NLOS propagation. Simulation results reveal that for relatively short distances, up to 1 m, data rates in the order of Tbps are obtained for a transmit power of 1 Watt. Moreover, the capacity of only the NLOS component is around 100 Gbps. These results are highly motivating to develop future wireless communication systems in the THz band which have ample research opportunities.

Acknowledgment: The work of Ian Akyildiz is supported by Alexander von Humboldt Foundation through his Humboldt Research Prize in Germany.

REFERENCES

- [1] H. Song and T. Nagatsuma, "Present and future of terahertz communications", *IEEE Transactions on Terahertz Science and Technology*, vol. 1, no. 1, pp. 256–263, 2011.
- [2] T. Rappaport, J. Murdock, and F. Gutierrez, "State of the art in 60-GHz integrated circuits and systems for wireless communications", *Proceedings of the IEEE*, vol. 99, no. 8, pp. 1390–1436, 2011.
- [3] IEEE-802.15-WPAN, "Terahertz Interest Group (IGthz)", 2014. [Online]. Available: <http://www.ieee802.org/15/pub/IGthzOLD.html>.
- [4] I. Akyildiz, J. Jornet, and C. Han, "Terahertz band: Next frontier for wireless communications", *Physical Communication*, vol. 12, pp. 16–32, 2014.
- [5] J. Jornet and I. Akyildiz, "Channel modeling and capacity analysis for electromagnetic wireless nanonetworks in the terahertz band", *IEEE Transactions on Wireless Communications*, vol. 10, no. 10, pp. 3211–3221, 2011.
- [6] R. Piesiewicz, T. Kleine-Ostmann, N. Krumbholz, D. Mittleman, M. Koch, and T. Kürner, "Terahertz characterisation of building materials", *Electronics Letters*, vol. 41, no. 18, pp. 1002–1004, 2005.
- [7] R. Piesiewicz, C. Jansen, S. Wietzke, D. Mittleman, M. Koch, and T. Kürner, "Properties of building and plastic materials in the THz range", *International Journal of Infrared and Millimeter Waves*, vol. 28, no. 5, pp. 363–371, 2007.
- [8] R. Piesiewicz, C. Jansen, D. Mittleman, T. Kleine-Ostmann, M. Koch, and T. Kürner, "Scattering analysis for the modeling of THz communication systems", *IEEE Transactions on Antennas and Propagation*, vol. 55, no. 11, pp. 3002–3009, 2007.
- [9] C. Jansen, S. Priebe, C. Moller, M. Jacob, H. Dierke, M. Koch, and T. Kürner, "Diffuse scattering from rough surfaces in THz communication channels", *IEEE Transactions on Terahertz Science and Technology*, vol. 1, no. 2, pp. 462–472, 2011.
- [10] S. Priebe, M. Jacob, C. Jansen, and T. Kürner, "Non-specular scattering modeling for THz propagation simulations", in *Proceedings of the 5th European Conference on Antennas and Propagation (EUCAP)*, IEEE, 2011, pp. 1–5.
- [11] P. Beckmann and A. Spizzichino, *The scattering of electromagnetic waves from rough surfaces*, A. House, Ed. 1987.
- [12] S. Priebe and T. Kürner, "Stochastic modeling of THz indoor radio channels", *IEEE Transactions on Wireless Communications*, vol. 12, no. 9, pp. 4445–4455, 2013.
- [13] Y. Choi, J. Choi, and J. Cioffi, "A geometric-statistic channel model for THz indoor communications", *Journal of Infrared, Millimeter, and Terahertz Waves*, vol. 34, no. 7-8, pp. 456–467, 2013.
- [14] M. Lawrence, "The relationship between relative humidity and the dewpoint temperature in moist air: A simple conversion and applications", *Bulletin of the American Meteorological Society*, vol. 86, no. 2, pp. 225–233, 2005.
- [15] L. Rothman, I. Gordon, Y. Babikov, A. Barbe, D. Benner, P. Bernath, M. Birk, V. Boudon, L. Brown, A. Campargue, J.-P. Champion, et al., "The HITRAN 2012 molecular spectroscopic database", *Journal of Quantitative Spectroscopy and Radiative Transfer*, vol. 130, no. 2013, pp. 4–50, 2013.
- [16] S. Nayar, K. Ikeuchi, and T. Kanade, "Surface reflection: physical and geometrical perspectives", *IEEE Transactions on Pattern Analysis and Machine Intelligence*, vol. 13, no. 7, pp. 611–634, 1991.
- [17] L. Kish, "Stealth communication: Zero-power classical communication, zero-quantum quantum communication and environmental-noise communication", *Applied Physics Letters*, vol. 87, no. 23, p. 234 109, 2005.
- [18] D. Tse, *Fundamentals of wireless communication*. Cambridge university press, 2005.